Lift-Off Dielectric Resonator for the Microwave Surface Resistance Measurement of Metal Plates

Samuel Hefford, Nicholas Clark, Richard Gumbleton and Adrian Porch

Abstract

A new method for accurate measurement of the microwave surface resistance of flat metal plates is proposed and verified experimentally, based on a sapphire dielectric resonator. System losses are accounted for by having continuous and controlled variation of the distance between the dielectric and the sample under test.

I. Introduction

THE surface impedance of a metal is defined to be the ratio of the tangential electric and magnetic fields at the surface. The real part of the surface impedance, i.e. the surface resistance R_S, quantifies the power loss per unit surface magnetic field and surface area. Hence, R_S determines the contribution to the power loss of the metal parts making up a passive microwave device. Currently, there is growing interest in the production of passive microwave components (in particular waveguides) using additive techniques [1]–[4]. Additive manufacture (AM) offers enhanced flexibility in design, enabling the realisation of complex geometries which would normally be difficult to produce. Additionally reductions in weight and profile can be achieved through part consolidation of the design, this has been identified as a cost saving measure for satellite antenna feed chains [3], [5].

For a hollow metal waveguide/cavity the power loss is dependant on the surface resistance (R_S) of the conductor. Optimum performance necessitates that we minimise loss in the system, and so R_S should also be minimised. This can be done by increasing conductivity of the conducting walls or by reducing surface roughness [6]–[9].

Current investigations into the microwave performance of AM surfaces have revolved around the manufacture of entire waveguide sections for testing [1]–[3]. The disadvantage to this approach is the cost and amount of time invested in producing just a single sample for testing. A more efficient method would be to measure the R_S of the surface directly using a dielectric resonator.

Dielectric resonators (or DRs) are a special case of microwave resonator where the electric and magnetic fields are closely confined to a dielectric piece, often shielded by a conducting cavity. Due to their low-loss, high Q, and small profile they have been used extensively to measure R_S in a variety of applications including high-temperature superconductors, graphene sheets, semiconductors, and copper-clad laminates [10]–[18]. Typically they consist of a single dielectric cylinder which is terminated at either one (open-ended) or both (Hakki-Coleman geometry) ends by a conducting sample. In some cases additional supports are used to position the dielectric within the structure.

Hakki-Coleman setups are often preferred as there are analytic solutions to the resonant field equations. This enables accurate determination of the geometric and energy-filling factors which are essential for R_S measurements [14], [19]. The main drawback to the Hakki-Coleman method is that two samples must be measured concurrently and the value of R_S found is the average of the two. In order to isolate a particular measurement a round robin approach can be employed; this greatly increases the number of measurements required [11], however these samples may then be kept as known standards for future measurements.

Open-ended setups are less commonly used as they do not have analytic solutions to the field equations; and so the geometric and energy-filling factors must be evaluated computationally [11]. Due to the widespread adoption of electromagnetic simulation packages, this is less of a concern. The main advantage is that unlike the Hakki-Coleman configuration, only a single sample is measured at a time.

In addition to the geometric and energy-filling factors, for both configurations the material loss parameters for the system components (walls, dielectric etc.) must be evaluated before any measurements can be made. Manufacturer values for the dielectrics loss tangent are sometimes used directly [18], and if known high temperature superconducting (HTS) film standards are available, these values can be verified [15]. More commonly the dielectric is measured in isolation using methods such as high order, quasi-TE_{0mn} modes [20] or whispering gallery modes [16]. These methods give very precise results at the cost of requiring an additional resonant structure.

We propose a new method for measuring the microwave surface resistance using a modified open-ended geometry and unique calibration approach. The novelty of this method is the ability to accurately determine the dielectric loss tangent *in situ* for an open-ended style dielectric resonator. This allows for the measurement of R_S for single sheets as opposed to the double sheets

required in the standard Hakki-Coleman configuration. Measurement results using this method have been published previously investigating the effect of build orientation in AM surfaces [21]. In this paper the theory of the method and measurement is expanded upon and a new resonator design is presented, operating in the C-band around 7.5 GHz. Finally results showing the potential accuracy are shown.

It should be declared that this paper reuses some content from thesis [22] with permission.

II. Theory

The modified open-ended dielectric resonator (referred to as lift-off dielectric resonator or LODR) is shown in Fig. 1. The LODR structure consists of a dielectric puck suspended from the top of a conducting cavity shield by a low-loss, low-permittivity dielectric rod. The main distinction of this structure from a traditional open-ended DR is that the rod is not fixed and is used to position the dielectric vertically. The base of the cavity can be removed and sample films or plates attached in its place for measurement. Two inductive coupling loops are used to make transmission measurements and the unloaded Q-factor and resonant frequency are evaluated using the Lorentzian curve fit method [23].

For measurement we chose to operate in the $\mathrm{TE}_{01\delta}$ dielectric resonator mode. This is done because at resonance circular currents are induced in the base plate, parallel to the interface between the base plate and the cylindrical outer wall. The advantage of this is that the measurement of R_S is not dependent on the pressure applied to this interface. Other modes with the electric and magnetic fields closely bound to the dielectric could also be used; however the discontinuity between the cavity walls and base would need to be considered.

Sample may be attached using screws, clips or simply placing the resonator atop the sample is also effective. This is especially true when using $\mathrm{TE}_{01\delta}$ as the measurement mode, as the surface currents will form closed loops and so will not be adversely affected by the join.

For illustration, the electric and magnetic field distributions for the $\mathrm{TE}_{01\delta}$ mode as well as surface currents induced at the baseplate are shown in Figs. 2 and 3. (Model used to produce plots is the same as that described later in Section III).

A. Static Equation for Q

The total loss of the LODR pictured in Fig. 1 can be separated into conductor losses (from the cavity walls and base) and dielectric losses (from the dielectric and the support rod). The unloaded Q (denoted as Q_0) can then be expressed as:

$$\frac{1}{Q_0} = \frac{1}{Q_{(walls)}} + \frac{1}{Q_{(base)}} + \frac{1}{Q_{(dielectric)}} + \frac{1}{Q_{(rod)}} \tag{1}$$

These losses can be defined in terms of R_S (conductors) and $\tan\delta$ (dielectrics) by geometric and energy-filling factors.

$$\frac{1}{Q_0} = \frac{G_w R_{Sw}}{f} + \frac{G_b R_{Sb}}{f} + p_d \tan\delta_d + p_r \tan\delta_r \tag{2}$$

where G_w and G_b are geometric factors associated with the cavity walls and base, p_d and p_r are energy-filling fractions associated with the dielectric and support rod, and f is the resonant frequency. For reference these factors are defined below and differ from the traditional definitions such as in [19] where frequency dependence has been abstracted.

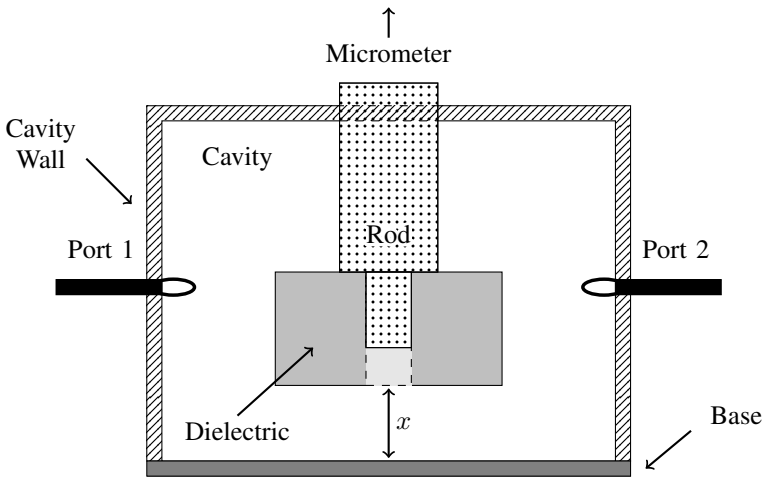

Fig. 1. Lift-Off Dielectric Resonator. The dielectric is held within a conducting cavity shield, which has a removable base plate. The dielectric position is manipulated vertically using a micrometer attached to the support rod. (Note: this diagram is illustrative only and does not have any dimensions associated with it.)

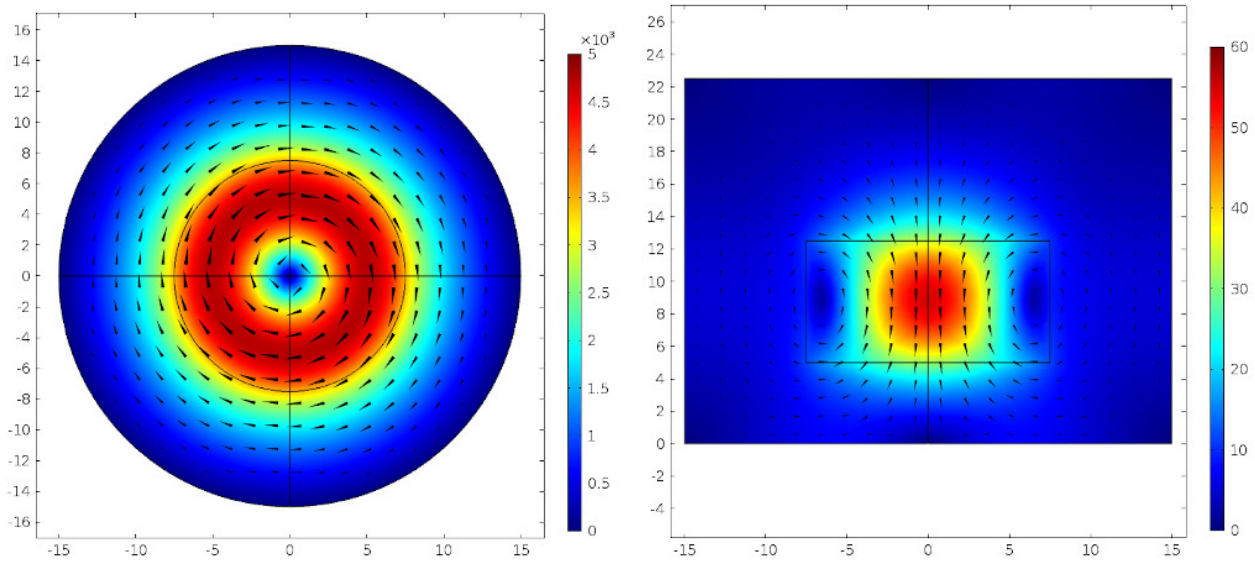

(a) Electric Field (V/m) (b) Magnetic Field (A/m)

Fig. 2. Electric and Magnetic field distributions for $TE_{01\delta}$ dielectric resonator mode at 6.82 GHz. Colour indicates field strength (red = high, blue = low). Dimensions for model are shown in millimetres.

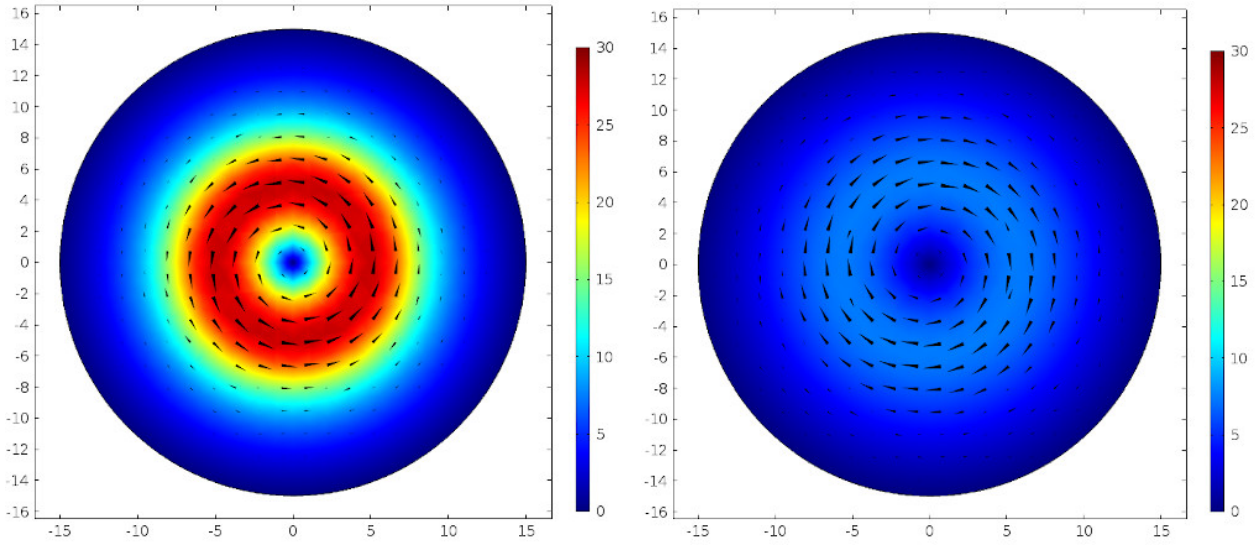

(a) Dielectric at base. (b) Dielectric at mid-point.

Fig. 3. Surface current density (A/m) at base plate for $TE_{01\delta}$ dielectric resonator mode at (a) 7.51 GHz and (b) 6.82 GHz. Colour scale maintained across both plots, arrows show vector field direction. Dimensions for model are shown in millimetres.

$$G_w = \Re\left(\frac{\oiint_{S_w} H_t \cdot H_t^* ds}{2\pi \iiint_V \mu H \cdot H^* dv}\right) \tag{3a}$$

$$G_b = \Re\left(\frac{\oiint_{S_b} H_t \cdot H_t^* ds}{2\pi \iiint_V \mu H \cdot H^* dv}\right) \tag{3b}$$

$$p_d = \Re\left(\frac{\iiint_{V_d} \varepsilon E \cdot E^* dv}{\iiint_V \varepsilon E \cdot E^* dv}\right) \tag{3c}$$

$$p_r = \Re\left(\frac{\iiint_{V_r} \varepsilon E \cdot E^* dv}{\iiint_V \varepsilon E \cdot E^* dv}\right) \tag{3d}$$

B. Lift-Off Equation for Q

It is well known that dielectric resonant modes are largely confined to the immediate area around the dielectric itself [24]. It should be clear then that as the dielectric lift-off position, x, is varied, the field distributions in the cavity will be modified giving rise to a change in both Q and f. This is similar to the results reported in [25] where dielectric height was varied to alter the frequency in a dielectric resonator. In this analysis however, we are altering the position of the dielectric *not* the dimensions.

Defining f_0, R_{S_0}, and $\tan\delta_0$ as the values of resonant frequency, surface resistance, and dielectric loss tangent when the dielectric is at the measurement point (e.g. $x = 0$ mm) allows the R_S and $\tan\delta$ to be defined in terms of frequency and their measurement point values.

$$R_S(f) = R_{S_0}\sqrt{\frac{f}{f_0}} \tag{4}$$

$$\tan\delta(f) = \tan\delta_0 \frac{f}{f_0} \tag{5}$$

Where (4) is given by rearrangement and simplification of (6) and (5) is an approximation for small changes in frequency.

$$R_S = \sqrt{\frac{\omega\mu}{2\sigma}} \tag{6}$$

Letting $f(x)$ be the resonant frequency as a function of x these results allow (2) to be re-written for any value of x as shown below.

$$\frac{1}{Q_0\,(x)} = \frac{G_w(x)R_{Sw_0}}{\sqrt{f(x)f_0}} + \frac{G_b(x)R_{Sb_0}}{\sqrt{f(x)f_0}} + \frac{p_d(x)\tan\delta_{d_0}}{f_0/f(x)} + \frac{p_r(x)\tan\delta_{r_0}}{f_0/f(x)} \tag{7}$$

This is the measurement equation and can be used to calculate the value of R_{Sb_0} at any point providing the values of R_{Sw_0}, $\tan\delta_{d_0}$, and $\tan\delta_{r_0}$ are known. The geometric and energy-filling factors have also been given an x dependency to account for the changing field distributions.

The change in f will be independent of loss and can be used to increase the accuracy of supplied values for permittivity in the simulation model. This is done by adjusting their values parametrically and comparing to measured data. To simplify this analysis, isotropic dielectric materials are preferred for both the dielectric resonator and the rod.

The LODR fixtures shown in this paper have been designed using either Nylon or PTFE for the rod and using Sapphire for the dielectric resonator. Nylon and PTFE are both isotropic materials and were chosen for their low relative real-part permittivity, (ε_r). Sapphire is anisotropic, however in the $\mathrm{TE}_{01\delta}$ mode there is only an azimuthal component to electric field which will purely be in the c-plane of the sapphire where $\varepsilon_r \approx 9.4$.

Once the values of ε_r for the dielectric resonator and rod have been fixed, the geometric and energy-filling factors can be evaluated with confidence at discrete points using (3).

C. Calibration Equation

For calibration a base plate made from the same material as the cavity shield is used. As they are the same material they will have the same conductivity and it can be assumed that at a given frequency their values for R_S will also be the same.

$$R_{Sw} = R_{Sb} \tag{8}$$

This simplifies (7) yielding the calibration equation where a maximum of three unknown variables must be solved for. In the ideal case the value of $p_r\tan\delta_r < 0.01$ always and the rod term can be omitted in the fit.

$$\frac{1}{Q\,(x)} = \frac{G_w(x) + G_b(x)}{\sqrt{f(x)f_0}} R_{Sw_0} + \frac{p_d(x)}{f_0/f(x)}\tan\delta_{d_0} + \frac{p_r(x)}{f_0/f(x)}\tan\delta_{r_0} \tag{9}$$

Calibration is then performed by least-squares curve fitting (9) to measured values of Q_0 over a range of x. Once calibration is done and the loss factors are known, measurement can be performed at any value of x within the calibrated range by replacing the base with the sample under test, measuring Q_0 at that point and then solving for R_{Sb_0} in (7).

III. Simulation Results

The accuracy and resolution of R_S measurements will depend on the degree to which the overall loss is influenced by the sample, and will be greatest when all but the sample losses are minimised [19]. To investigate this a number of simulations were performed using COMSOL multi-physics. These were done in order to quantify the accuracy of the LODR method, and also to identify any factors influencing accuracy which could be improved. This gave the advantage that loss factors found through calibration could be compared to the actual values used in the simulation model. This eliminated the need for secondary measurements and helped to establish a theoretical accuracy.

The choice of support rod material was investigated for its impact on calibration accuracy and also the effect of different sample conductivities and measurement lift-off positions on measurement accuracy.

A. Simulation Model

Two LODR models were set up using the same dimensions, one with a support rod and one without. The cavity walls were set to use Aluminium, and c-plane sapphire was set as the dielectric material. For the support rod model two materials were investigated: Nylon and PTFE. The dimensions for both are shown in Fig. 4, and material definitions are given in Tab. I.

No surface roughness is considered in the simulation model, and so R_S comes out as in (6) for an ideal flat conductor. For real samples the measured R_S value should be considered an effective value; modified from the nominal value by the presence of any surface roughness.

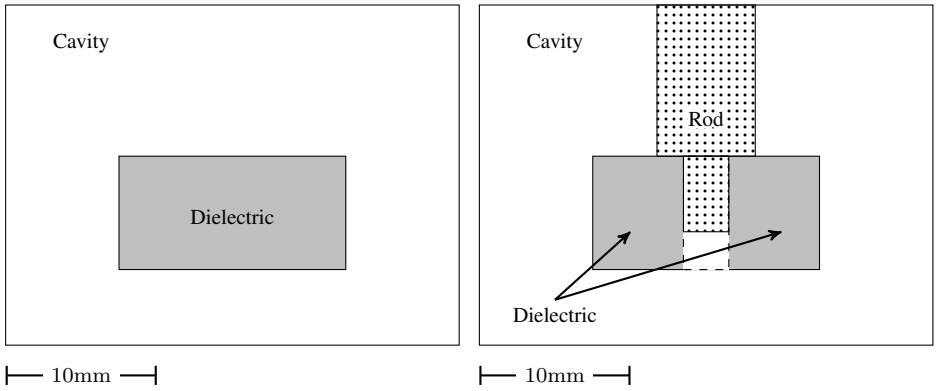

(a) Model without Rod. (b) Model with Rod.

Fig. 4. LODR geometries used for simulation. Geometries are shown as cross-sections with rotational symmetry about the z-axis. Images are to scale.

TABLE I
COMSOL Material Definitions

Material	ε_r [1]	$\tan\delta^\dagger$ [1]	μ_r [1]	σ [S/m]
Air	1.00	0.00	1.00	0.00
Aluminium	1.00	-	1.00	2.86×10^7
Nylon	2.90	1.20×10^{-2}	1.00	0.00
PTFE	2.10	1.50×10^{-4}	1.00	0.00
Sapphire	9.40	3.00×10^{-5}	1.00	0.00

†Value at 10 GHz

B. Calibration Accuracy

Calibration was simulated using a parametric sweep which varied the lift-off value (x) from 0-5 mm in 0.1 mm steps. At each point, frequency, Q_0 and the loss tangents were evaluated for the $TE_{01\delta}$ resonant mode. Electric and Magnetic field integrals were also taken and the geometric and energy-filling factors were calculated using the integrals defined in (3) for all three models (no rod, nylon rod, PTFE rod).

Calibration was performed by non-linear least-squares fitting of the calibration equation (9) to the value of Q_0 evaluated through simulation in Matlab. A reduced version of (9) was used for the no rod model where the support rod term was omitted. Calibration was repeated multiple times using each value of x simulated for the reference point (x_0). Calibration error was calculated as the absolute deviation of the fitted loss value from the true value used by the model as a percentage.

TABLE II
CALIBRATION ACCURACY

Model	Parameter	Value	Fit	Error (%)
No Rod	R_{sw0} (Ω)	3.24×10^{-2}	3.25×10^{-2}	0.49
	$\tan\delta_{d_0}$ (1)	2.27×10^{-5}	2.27×10^{-5}	0.09
PTFE	R_{sw0} (Ω)	3.24×10^{-2}	3.26×10^{-2}	0.84
	$\tan\delta_{d_0}$ (1)	2.28×10^{-5}	2.29×10^{-5}	0.87
	$\tan\delta_{r_0}$ (1)	1.14×10^{-4}	1.45×10^{-10}	-
Nylon	R_{sw0} (Ω)	3.23×10^{-2}	3.44×10^{-2}	6.25
	$\tan\delta_{d_0}$ (1)	2.27×10^{-5}	2.56×10^{-5}	12.5
	$\tan\delta_{r_0}$ (1)	9.10×10^{-3}	8.21×10^{-3}	9.72

Reference point used (x_0) : $0.10\mathrm{mm}$

Calibration error was found to be constant regardless of reference point used, and the result for $x_0 = 0.1\mathrm{mm}$ is given in Tab. II. The error for the no rod model was lower than that of the PTFE model, which itself was lower than for the Nylon model. Ignoring $\tan\delta_{r_0}$ the overall error in fit for PTFE model was very low. The large error for $\tan\delta_{r_0}$ indicates under-fitting due to low impact on Q; examination of its percentile contribution to loss confirmed it as negligible ($< 1\%$). Repeating the calibration for the PTFE model using the reduced 2-parameter calibration yielded the same values for R_{Sw0} and $\tan\delta_{d_0}$. This was not the case for the Nylon model, where the value of $\tan\delta_{r_0}$ gave a significant contribution to loss such that omitting the term gave a tenfold increase in percentile error.

These results indicated that greatest accuracy can be achieved by selecting a material for the support rod such that its contribution to loss is negligible, allowing it to be omitted from the fit altogether.

C. Measurement Accuracy: Sample Conductivity

In this simulation measurements were simulated using a parametric sweep where the value of base (or sample) conductivity was swept from 1.0×10^7 to 10.0×10^7 $\mathrm{S\,m^{-1}}$ in 1.0×10^7 steps. This range includes most metals at room temperature, with Ag having the highest conductivity around 6.3×10^7 $\mathrm{S\,m^{-1}}$, common AM alloys also fall within this range. Measurement position was fixed as $x = 0.10\mathrm{mm}$ and sample R_s were evaluated using the calibration results from Tab. II. Measurement error was calculated as the absolute difference between measured value and the theoretical value of R_s expressed as a percentage of the theoretical value. Theoretical values were calculated using the conductivity and frequency defined in the simulation. These results are shown in Fig. 5.

Measurement error was seen to increase with sample conductivity for both the Nylon and PTFE rod models. For greatest measurement accuracy the loss term from the sample must dominate [19]. An increasing sample conductivity acts to reduce its loss term, making it more susceptible to measurement error. For the same reason the measurement error for the Nylon rod model was also higher; where the value of $\tan\delta$ for Nylon was substantially higher than for PTFE, reducing sensitivity of the measurement to the sample loss term.

In the no-rod model no such dependency on conductivity was observed, likely due to insufficient mesh simulation. This would also explain the less orderly trend seen in the PTFE data as compared to Nylon.

The results for the PTFE model demonstrate that reasonable accuracy of around 1% error can be achieved, even for high conductivity metals (e.g. Gold, Copper, Silver).

D. Measurement Accuracy: Measurement Position

In this simulation measurements were simulated using a parametric sweep where the measurement position, x_0, was swept from 0 to 4.5 mm in 0.5 steps. Sample conductivity was fixed as $\sigma = 1.0 \times 10^8 \mathrm{S\,m^{-1}}$, sample R_S was evaluated using the calibration results from Tab. II. Measurement error was calculated by comparing the evaluated value of R_S for the base with the theoretical value calculated from the conductivity and frequency defined in the simulation. These results are shown in Fig. 6.

As can be seen measurement error was shown to increase with measurement position in all three models. As previously mentioned measurement accuracy is dependent on the dominance of the sample loss term. In a dielectric resonator the electric and magnetic fields for the $\mathrm{TE}_{01\delta}$ mode are tightly confined to the dielectric, thus increasing the distance between sample and dielectric will decrease the magnetic field magnitude at the sample. This means that as measurement position is moved further from the base the loss term associated with the sample is diminished and with it the measurement accuracy. Thus for optimal results, measurements should be taken with the dielectric at the base.

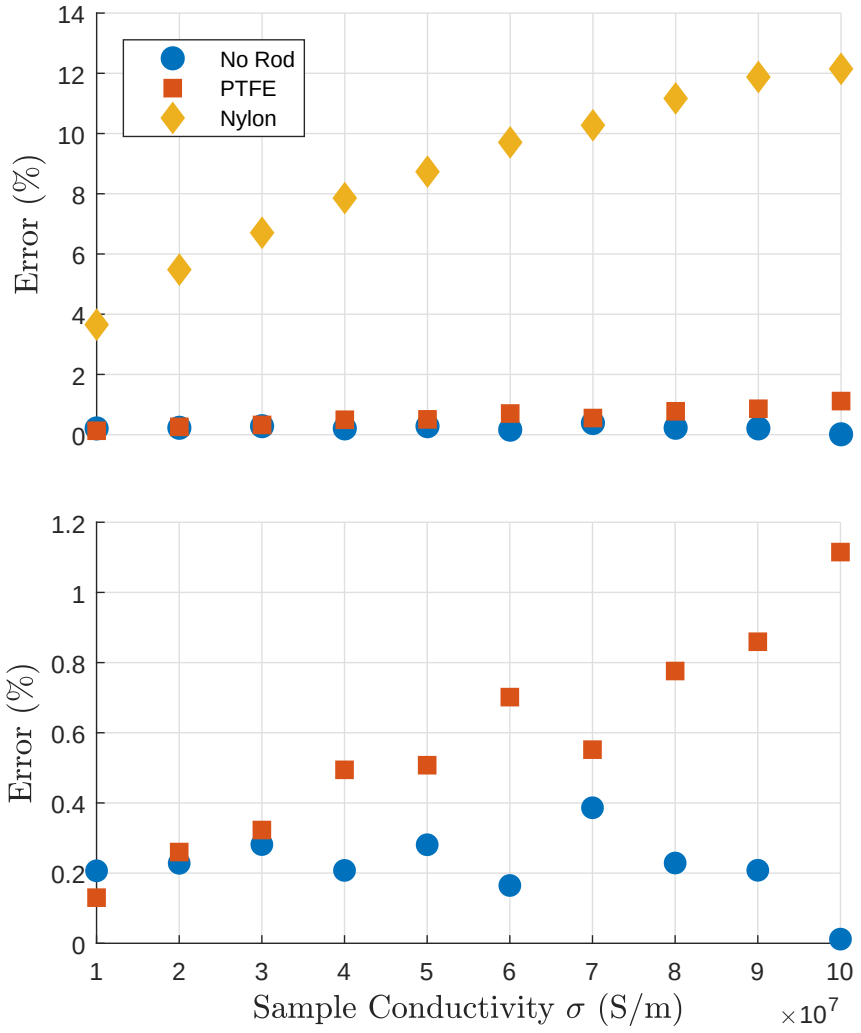

Fig. 5. Absolute measurement error for increasing sample conductivities. Measurement error calculated as absolute deviation of LODR evaluated value of R_S from the true value expressed as a percentage.

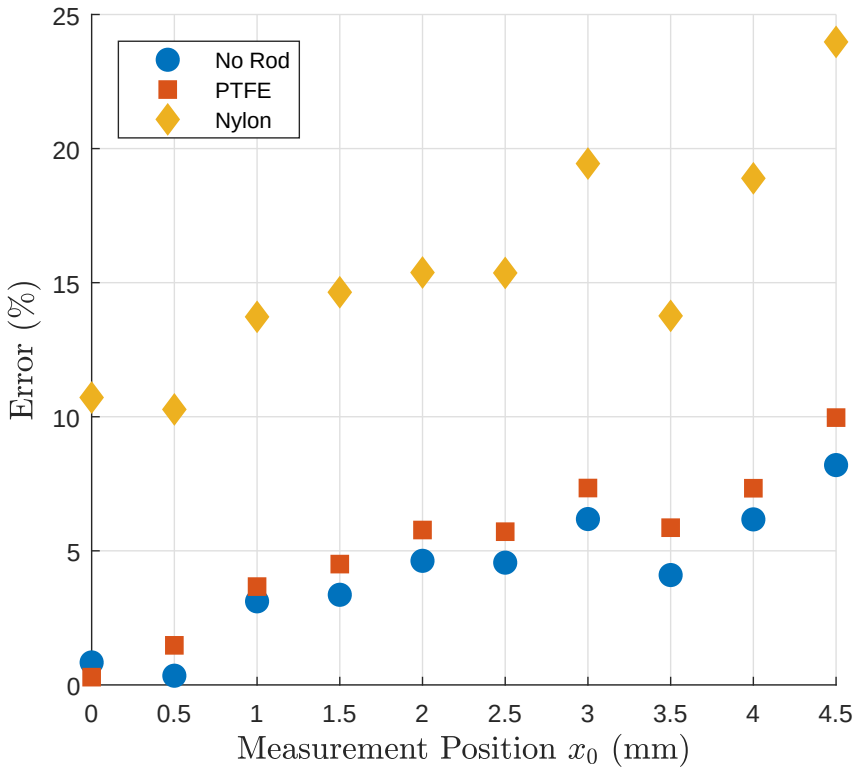

Fig. 6. Absolute measurement error for increasing measurement position. Measurement error calculated as absolute deviation of LODR evaluated value of R_S from the true value expressed as a percentage.

IV. C-Band Lift-Off Dielectric Resonator

A. Design

The LODR fixture shown in Fig. 7 was designed to operate in the $TE_{01\delta}$ mode in the c-band. The resonant frequency was measured as 7.58 GHz with the dielectric at the base (i.e. $x = 0$ mm). Single-crystal c-plane sapphire was used for the dielectric which has a $\tan\delta$ of around 1×10^{-5} at 10 GHz and room temperature [26]. The cavity shield was machined from aluminium and the support rod was made from PTFE. A micrometer head was affixed to the support rod for accurate manipulation of the dielectric height.

Fig. 7. C-band LODR fixture operating in the $TE_{01\delta}$ mode around 7.58 GHz with dielectric at the base (i.e. $x = 0$mm). Coupling is achieved inductively by two loop-terminated SMA ports.

The cavity shield and dielectric dimensions were selected to avoid interference of adjacent modes to the measurement mode over the lift-off range. As a precaution a minimum separation of 300 MHz around the measurement mode was enforced. The frequency distribution of resonant modes is shown in Fig. 8 over a 5 mm lift-off range. The cavity shield had an internal radius of 15 mm and a height of 22.5 mm. The dielectric had a 7.5 mm radius and a height of 7.5 mm.

B. Calibration

For calibration a base plate was machined from the same grade of aluminium as the cavity shield. Transmission (S_{21}) measurements were made over a lift-off range of 2 mm at 0.1 mm increments using a PNA series Agilent vector network analyser, connected to the resonator by inductive loop-terminated coaxial connectors. Lorentzian curve fitting was used to evaluate the values of f_0 and Q_0 for each measurement, and geometric and energy-filling factors were evaluated through simulation using COMSOL multiphysics.

Calibration was performed using (9) and the results of the curve fit are shown in Fig. 9 and Tab. III.

TABLE III
Calibration Result

Parameter	3-Parameter Fit	2-Parameter Fit	Units
R_{S_0}	3.04×10^{-2}	3.39×10^{-2}	Ω
$\tan\delta_{d_0}$	1.89×10^{-5}	2.22×10^{-5}	1
$\tan\delta_{r_0}$	1.90×10^{-3}	- -	1

($x_0 = 0.10$mm, $f_0 = 7.54$GHz)

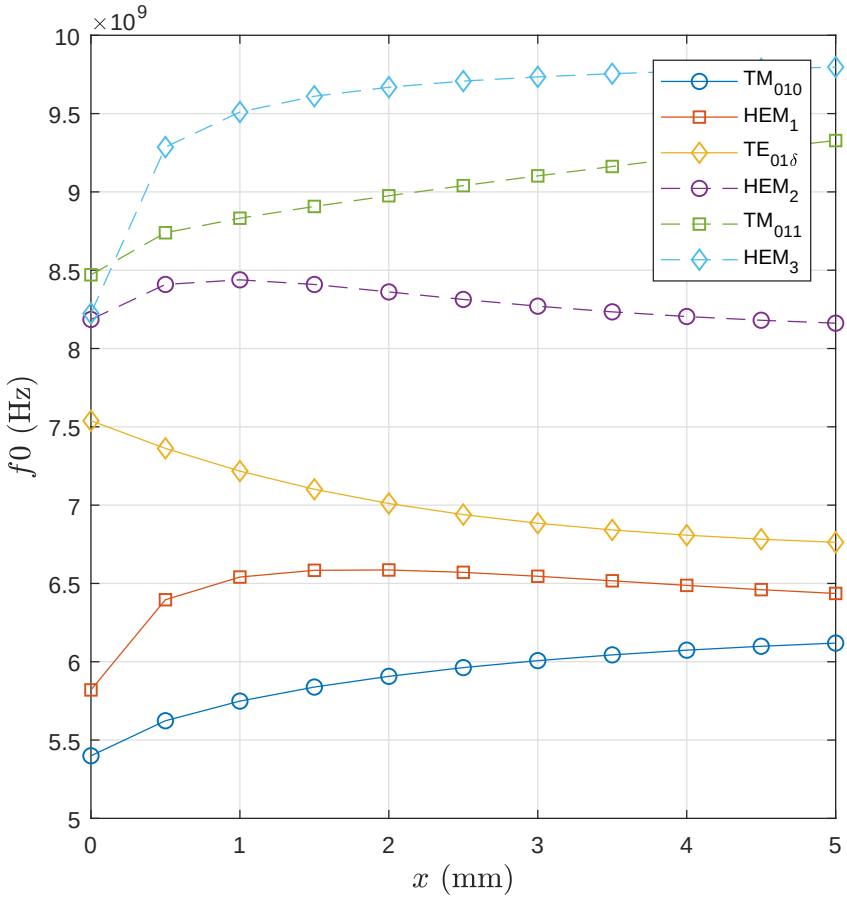

Fig. 8. Resonant mode frequency distribution for LODR fixture over a 5 mm lift-off range. Hybrid modes are labelled as HEM and are numbered arbitrarily in order of increasing frequency at $x = 5$ mm.

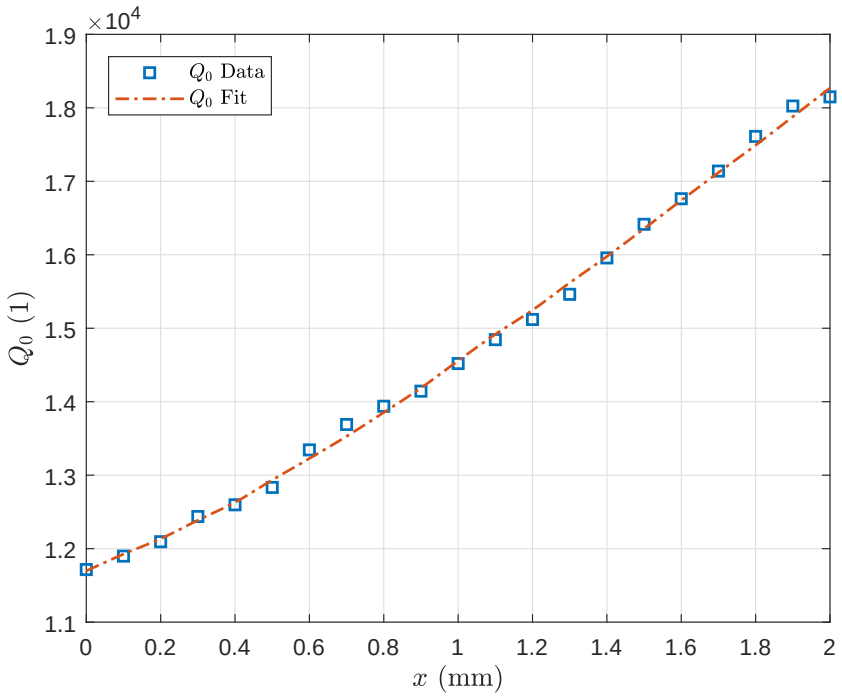

Fig. 9. Measured Q_0 and LSQ fitted Q_0 versus lift-off position, x. Good agreement between measured and fitted results was achieved using 2-parameter calibration equation.

V. Measurements of Sheet and AM Metal Surfaces

In order to assess the accuracy of the C-band LODR fixture samples of 316L Stainless Steel and AlSi10Mg Aluminium were measured. Samples of guillotine cut sheets were prepared along with additively manufactured samples produced vertically by powder-bed fusion (PBF) on a Renishaw AM250 additive manufacture system. PBF samples were also grit-blasted.

Sample dimensions were approximately 60×60 mm. Transmission (S_{21}) measurements were made at a lift-off of 0.1 mm using a PNA series Agilent vector network analyser, connected to the resonator by inductive loop-terminated coaxial connectors. Lorentzian curve fitting was used to evaluate the values of f_0 and Q_0 for each measurement. Mounting holes were present on PBF samples; however, all measurements in this study were made with the LODR fixture resting on top. For illustration Fig. 10 shows an image of the 316L sheet and PBF samples.

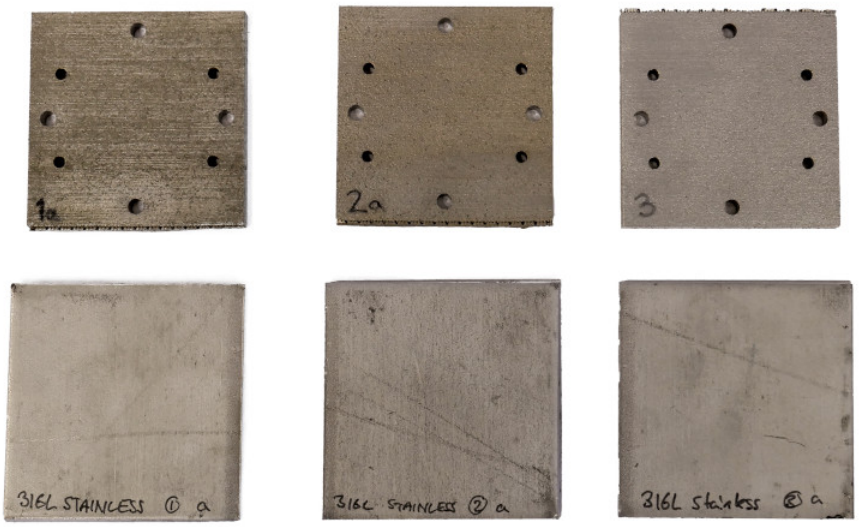

Fig. 10. 316L Stainless Steel Samples. Top: PBF plates produced in vertical configuration. Bottom: Stock metal plates guillotine cut from same sheet. Image manipulation carried out to remove background.

Values of R_S were evaluated for each surface type using the calibration result in Tab. III. A total of 3 samples were measured for both PBF and sheet for each material, and the mean average and sample standard deviation have been plotted in Fig. 11. The theoretical value of R_S at the measurement frequency for each material are also shown. The values for conductivity used to calculate these were 2.17×10^7 and 1.35×10^6 $\mathrm{S\,m^{-1}}$ for AlSi10Mg and 316L, respectively.

As can be seen, the measurements of the guillotine cut sheets were in close agreement to the theoretical values. Notably the AlSi10Mg sheet was closer in value to its theoretical than the 316L; a possible explanation could be the visible tarnishing on the 316L surface as can be seen in Fig. 10. As 316L is a stainless steel this is unlikely to be oxidation and may instead be evidence of surface roughness which is known to influence R_S [7]–[9].

Given that the sheet samples were all cut from the same sheet, the small standard deviation between samples gives an encouraging indicator for the precision of this measurement. The close proximity to theoretical value also gives an encouraging result for accuracy. Without having a standard surface of known R_S to use it is difficult to comment on the absolute accuracy; however, if one were to consider the AlSi10Mg to be "good-enough" then accuracy could be quoted to 5×10^{-3} Ω at that conductivity and measurement position.

As might be expected the PBF surfaces performed worse than the sheet samples for both materials, with R_S being almost 50% greater than their sheet counterparts on average. There was a greater standard deviation in the 316L samples compared to the AlSi10Mg samples, despite them having the same processing conditions (vertical orientation, grit-blasted). The fact that AlSi10Mg gave a more consistent surface than the 316L is a surprising result considering 316L is one of the most commonly used powders for metal PBF.

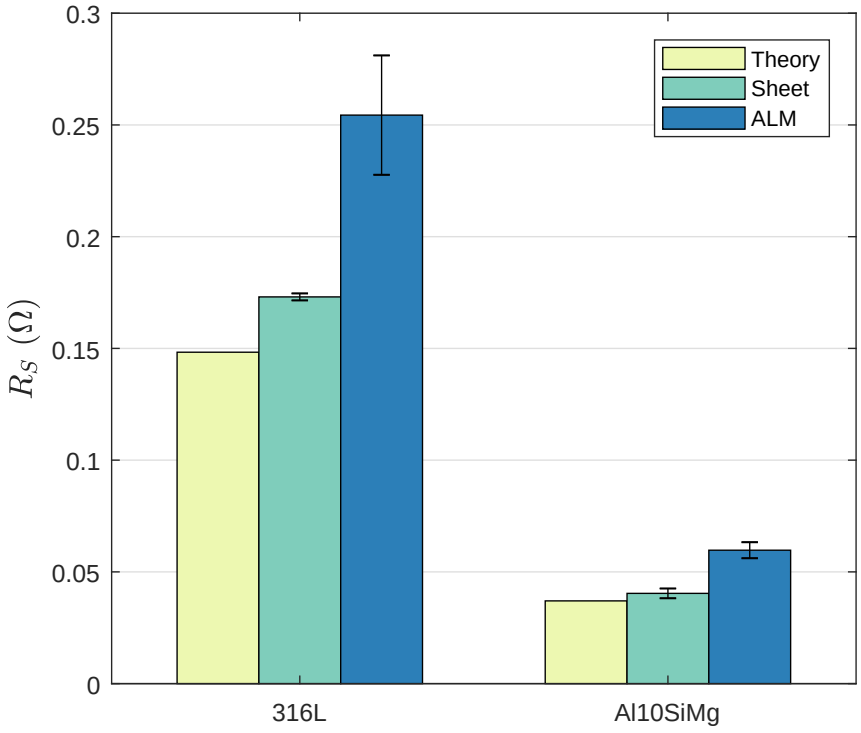

Fig. 11. Measured R_S of 316L stainless steel and AlSi10Mg aluminium. Values plotted are the arithmetic mean of the R_S evaluated for three separate samples. Error bars indicate the sample standard deviation.

VI. Conclusions

A new calibration technique has been introduced for determining parasitic system losses of a dielectric resonator. The method (shown previously in [21]) utilises a novel dielectric resonator structure. The dielectric position is manipulated in order to provide a characteristic change in Q to which a calibration equation can be fit, and the parasitic system losses extracted.

Simulation results were presented which assessed the potential accuracy of the method. As is well-known [19] measurement accuracy was dependant on the dominance of the loss term associated with the sample, in the case of the lift-off dielectric resonator this was shown for sample conductivity and measurement position.

The design of a LODR operating in the C-band was presented, along with its calibration result. The presented fixture was designed to operate in the $\mathrm{TE}_{01\delta}$ resonant mode at a frequency of 7.58 GHz. This mode was selected to overcome the anisotropy of the c-plane sapphire used for the dielectric.

Measurements of guillotine cut sheet and PBF surfaces were presented for 316L Stainless Steel and AlSi10Mg Aluminium. Overall it was shown that the sheet measurements were in close agreement with their theoretical value for R_S, while the PBF samples tended to have a higher value of R_S. While it is difficult to comment on absolute accuracy due to the non-existence of a standard surface; if one were to assume the AlSi10Mg samples to be sufficient, then a minimum accuracy of 5×10^{-3} Ω at that conductivity and measurement position may have been achieved.

Finally, note that we have not considered surface roughness in our analysis. For that reason, one might consider the values of R_S produced to be effective ones, dependent on both the electrical properties and roughness of the surface, especially since this is on a scale greater than the expected skin depth.

In future work, we propose to use the LODR to study the effects of post processing on the surface resistance of AM manufactured metal plates, and other factors linked to the AM process; these include build orientation and any surface texturing produced by the laser beam scanning protocol.

Acknowledgements

The authors wish to acknowledge EPSRC for funding via its iCASE award in partnership with Renishaw Plc.

Data supporting the results reported in this paper are openly available from the Cardiff University catalogue at http://doi.org/10.17035/d.202

REFERENCES

[1] P. Booth, J. Gilmore, E. V. Lluch, and M. Harvey, "Enhancements to satellite feed chain performance, testing and lead-times using additive manufacturing," in *2016 10th European Conference on Antennas and Propagation (EuCAP)*, Apr. 2016, pp. 1–5.

[2] J. Lorente, M. Mendoza, Z. Petersson, L. Pambaguian, Melcon, and C. Ernst, "Single part microwave filters made from selective laser melting," in *Proceedings of the 39th European Microwave Conference*, 2009, pp. 1421–1424.

[3] O. A. Peverini, M. Lumia, F. Calignano, G. Addamo, M. Lorusso, E. P. Ambrosio, D. Manfredi, and G. Virone, "Selective laser melting manufacturing of microwave waveguide devices," *Proceedings of the IEEE*, vol. 105, no. 4, pp. 620–631, Apr. 2017.

[4] H. Yukawa, Y. Ushijima, M. Abe, N. Yoneda, and M. Miyazaki, "A metal 3d-printed t-junction omt with an offset stepped post," in *Proceedings of the 47th European Microwave Conference*, 2017, pp. 444–447.

[5] T. Duda and L. V. Raghavan, "3d metal printing technology: the need to re-invent design practice," *AI and Society*, vol. 33, no. 2, pp. 241–252, May 2018.

[6] T. Y. Otoshi and M. M. Franco, "The electrical conductivities of steel and other candidate materials for shrouds in a beam-waveguide antenna system," *IEEE Transactions on Instrumentation and Measurement*, vol. 45, no. 1, pp. 77–83, Feb. 1996.

[7] B. Curran, I. Ndip, S. Guttowski, and H. Reichl, "On the quantification and improvement of the models for surface roughness," *2009 IEEE Workshop on Signal Propagation on Interconnects*, 2009.

[8] K. Pitt, C. Free, Z. Tian, and M. Jakubowska, "A method for the prediction of microwave properties of thick film conductors from physical measurements and d.c. conductivity," *Journal of Materials Science: Materials in Electronics*, vol. 12, no. 9, pp. 491–495, 2001.

[9] E. Hammerstad and O. Jensen, "Accurate models for microstrip computer-aided design," *MTT-S International Microwave Symposium Digest*, vol. 80, no. 1, pp. 407–409, 1980.

[10] V. J. Krupka, M. Klinger, M. Kuhn, A. Baranyak, M. Stiller, J. Hinken, and J. Modelski, "Surface resistance measurements of hts films by means of sapphire dielectric resonators," *IEEE Transactions on Applied Superconductivity*, vol. 3, no. 3, pp. 3043–3048, 1993.

[11] J. Mazierska, "Dielectric resonator as a possible standard for characterization of high temperature superconducting films for microwave applications," *Journal of Superconductivity*, vol. 10, no. 2, pp. 73–84, Apr. 1997.

[12] W. Diete, M. Getta, M. Hein, T. Kaiser, G. Muller, H. Piel, and H. Schlick, "Surface resistance and nonlinear dynamic microwave losses of epitaxial hts films," *IEEE Transactions on Applied Superconductivity*, vol. 7, no. 2, pp. 1236–1239, Jun. 1997.

[13] N. J. Parker, A. P. Kharel, J. R. Powell, P. A. Smith, P. D. Evans, and A. Porch, "Measurements and modeling of hts shielded dielectric resonators," *IEEE Transactions on Applied Superconductivity*, vol. 9, no. 2, pp. 1928–1931, 1999.

[14] J. Mazierska and C. Wilker, "Accuracy issues in surface resistance measurements of high temperature superconductors using dielectric resonators (corrected)," *IEEE Transactions on Applied Superconductivity*, vol. 11, no. 4, pp. 4140–4147, Dec. 2001.

[15] M. V. Jacob, J. Mazierska, K. Leong, D. Ledenyov, and J. Krupka, "Surface resistance measurements of hts thin films using slao dielectric resonator," *IEEE Transactions on Applied Superconductivity*, vol. 13, no. 2, pp. 2909–2912, Jun. 2003.

[16] J. Krupka, "Measurements of the surface resistance and the effective conductivity of copper cladded laminates employing dielectric resonator technique," pp. 515–518, 2007.

[17] J. Krupka and J. Mazierska, "Contactless measurements of resistivity of semiconductor wafers employing single-post and split-post dielectric-resonator techniques," *IEEE Transactions on Instrumentation and Measurement*, vol. 56, no. 5, pp. 1839–1844, Oct. 2007.

[18] O. Shaforost, K. Wang, S. Goniszewski, M. Adabi, Z. Guo, S. Hanham, J. Gallop, L. Hao, and N. Klein, "Contact-free sheet resistance determination of large area graphene layers by an open dielectric loaded microwave cavity," *Journal of Applied Physics*, vol. 117, no. 2, p. 24501, 2015.

[19] J. Krupka and J. Mazierska, "Improvement of accuracy in measurements of the surface resistance of superconductors using dielectric resonators," *IEEE Transactions on Applied Superconductivity*, vol. 8, no. 4, pp. 164–167, 1998.

[20] J. Krupka, Ł. Usydus, and H. Kołtuniak, "Sheet resistance and conductivity measurements of rough surfaces of metals on printed circuit boards and metalized ceramic substrates," pp. 149–153, 2012.

[21] N. Clark, S. Hefford, and A. Porch, "Effect of build orientation and surface finish on surface resistance in microwave components produced by selective laser melting," in *Proceedings of the 47th European Microwave Conference Monitoring*, 2017, pp. 2–5.

[22] S. Hefford, "Microwave processing in additive manufacturing," PhD Thesis, Cardiff University, 2019.

[23] P. J. Petersan and S. M. Anlage, "Measurement of resonant frequency and quality factor of microwave resonators: Comparison of methods," *Journal of Applied Physics*, vol. 84, no. 6, pp. 3392–3402, 1998.

[24] D. Kajfez and P. Guillon, *Dielectric Resonators*, 2nd ed., ser. Noble Publishing Classic Series. Noble Publishing Corporation, 1998.

[25] I. S. Ghosh, D. Schemion, and N. Klein, "Temperature compensated high-q dielectric resonators for long term stable low phase noise oscillators," in *Proceedings of International Frequency Control Symposium*, May 1997, pp. 1024–1029.

[26] J. G. Hartnett, M. E. Tobar, E. N. Ivanov, and J. Krupka, "Room temperature measurement of the anisotropic loss tangent of sapphire using the whispering gallery mode technique," *IEEE Transactions on Ultrasonics, Ferroelectrics, and Frequency Control*, vol. 53, no. 1, pp. 34–38, 2006.

Samuel Hefford received the BEng (Hons.) degree in Electronic and Communications Engineering and PhD degree in Microwave Engineering from Cardiff University, UK. His research utilises microwave resonant structures and involves the development of measurement and processing techniques for metal powder compacts and additive surfaces. He currently works as a research associate at Cardiff University in the Centre for High-Frequency Engineering.

Nicholas Clark received the BEng (Hons.) degree in Computer Systems Engineering and PhD degree in Microwave Engineering from Cardiff University, UK. His research involved the application of microwave resonant structures and his specific interests include the characterisation and heating of metal powders and structures and the development of precision microwave heating systems. He currently works as a Control and Analysis engineer for YASA Ltd based in Oxford, UK.

Richard Gumbleton received the BEng (Hons.) degree in Electronic and Communications Engineering from Cardiff University, UK in 2017. He is currently a PhD student studying Microwave Engineering at Cardiff University as part of an iCASE studentship with Renishaw Plc. His research interests include additive manufacturing for microwave applications, specifically the characterisation and optimisation of additively manufactured surfaces.

Adrian Porch is a full professor in the School of Engineering at Cardiff University and the research leader of the Center for High Frequency Engineering. He has been at Cardiff since 2000 and previously was an academic in the School of Electronic and Electrical Engineering at Birmingham University, U.K. (1990-2000). He read Natural Sciences (Physics, MA, 1983-1986) and Low Temperature Physics (PhD, 1986-1989) at Cambridge University, U.K. He has published over 150 papers in the area of the high frequency properties and applications of materials. His recent research has diversified into medical applications using microwave technology.